

Modeling of heat and mass transfer in direct contact membrane distillation: effect of counter diffusion velocity

Hesam Bazargan Harandi^a, Anahita Asadi^a, Zuguo Shen^a, Mohammad Rahnama^b, Ned Djilali^b, Pang-Chieh Sui^{a,*}

^aSchool of Automotive Engineering, Wuhan University of Technology, Wuhan 430070, China, emails: pcsui@whut.edu.cn (P.-C. Sui), hbazargan@whut.edu.cn (H.B. Harandi), anahita.asadi@whut.edu.cn (A. Asadi), shenzuguo@whut.edu.cn (Z. Shen)

^bInstitute for Integrated Energy Systems and Department of Mechanical Engineering, University of Victoria, Victoria BC V8W 2Y2, Canada, emails: rahnama@uvic.ca (M. Rahnama), ndjilali@uvic.ca (N. Djilali)

Received 9 May 2020; Accepted 4 November 2020

ABSTRACT

Membrane distillation is a non-isothermal separation process that uses a porous hydrophobic membrane. Water in the hot feed stream diffuses through the membrane in the form of vapor and condenses on the cold permeate side. Inside the porous membrane, the diffusion of water vapor is accompanied by the counter diffusion of air, which is often ignored in most studies. In this study, the role of counter diffusion velocity in a flat-sheet membrane contactor is analyzed using a two-dimensional model of direct-contact membrane distillation with a counter-flow configuration. Considering such a counter diffusion velocity, the simulation results of the total flux showed improved prediction accuracy in relation to experimental data in comparison with that in previous studies. The effects of different parameters, including feed inlet temperature and linear velocity, on gain output ratio (GOR), and transmembrane flux were investigated in detail. Our results indicate that an increase in the feed inlet temperature increases the total flux significantly. It is revealed that a higher linear velocity reduces the heat transfer resistance, which lowers the difference between the bulk and membrane interface temperatures. It was found that increases in both the feed inlet temperature and linear velocity enhanced the GOR. Using a sensitivity analysis, it was observed that membrane thickness had the strongest influence on the GOR and temperature polarization coefficient.

Keywords: Direct contact membrane distillation; Counter diffusion velocity; Gain output ratio; Transmembrane flux; Temperature polarization

1. Introduction

Human life and all agricultural and industrial developments depend on water as a vital resource. According to the United Nations, only 2.5% of the total volume of water on the earth is freshwater [1]. The increasing global population and demand for higher standards of living have made water scarcity a main challenge for human beings. In recent decades, saltwater desalination has been used as the main source of potable water in many countries [1–3]. Membrane distillation (MD), which utilizes a hydrophobic, porous

polymer membrane to extract fresh water from hot brines, has emerged as a promising approach for large-scale desalination processes in the near future owing to some important advantages, for example, lower operating temperature and capability to treat more concentrated brines in comparison with other desalination systems. Furthermore, MD is not only an appropriate method for producing freshwater but is also suitable for various applications that require the separation of liquids in the medical, pharmaceutical, and food industries and for wastewater treatment. Another advantage of MD in comparison with other desalination

* Corresponding author.

systems is that solar energy can be employed to supply the energy required to maintain the operating temperature of the feed water in the range between 30°C and 90°C [4]. In addition, waste heat harvested from cogeneration systems can be used as the heat source for MD.

The technical complexity of MD systems is lower than that of other desalination technologies, such as multi-stage flash (MSF) and multi-effect desalination (MED) using vacuum stages [5,6]. In an MD system, a vapor pressure gradient across the membrane, which acts as the main driving force, is established in different ways. Most common configurations, such as direct contact membrane distillation (DCMD), utilize a temperature difference as the driving force. In DCMD, both the feed and permeate channels are in direct contact with the membrane [7]. For continuous production of freshwater, the feed solution is heated and the permeate is cooled in external heat exchangers and then actively circulated parallel to the membrane. DCMD has been investigated extensively by researchers using commercial hydrophobic membranes of polytetrafluoroethylene (PTFE), polypropylene (PP), and polyvinylidene fluoride (PVDF). The hydrophobic nature of the membranes prevents capillary condensation and membrane wetting.

Most studies on DCMD to date have been experimental works, although there has been a significant increase in modeling activity for DCMD recently. Lawson and Lloyd [8] reported the membrane properties and mass transfer phenomena in detail. Schofield et al. [9] presented a mathematical model for the simulation of DCMD and investigated factors affecting the flux of distilled water. Khayet et al. [10] proposed a theoretical model including membrane characteristics and heat and mass transfer mechanisms to estimate the thickness of the hydrophobic layer made of porous composite membranes. Andrjesdóttir et al. [11] compared the accuracies of different heat transfer prediction methods in combination with the three different forms of the dusty gas model for mass transport in laminar and turbulent flow regimes under steady-state conditions. Winter [12] employed comprehensive mathematical models for different types of MDs, such as DCMD, permeate gap membrane distillation (PGMD), air gap membrane distillation (AGMD), vacuum membrane distillation (VMD), and sweeping gas membrane distillation (SGMD), to conduct module evaluations, which may be used for techno-economic optimization of the module, including multi-objective optimization. In addition, this comprehensive study investigated the effect of Knudsen, ordinary molecular diffusion, and viscous flow on mass transport through the membrane pores.

Khayet and Matsuura [13] proposed another method for the simulation of DCMD, which is based on the development of transport models based on the resistance-in-series theory. This method reveals the impacts of key parameters that affect the performance of DCMD. Furthermore, a Monte Carlo simulation model was developed to study the vapor flux through the hydrophobic membranes used in DCMD. The Monte Carlo models were designed without using any adjustable parameters, and the membrane pore space was described by a three-dimensional network of interconnected cylindrical pores with size distribution and nodes. Manawi et al. [14] suggested a predictive model for the assessment of the temperature polarization effect in

DCMD desalination of high-salinity feed. They obtained the local temperature polarization coefficient, while others used the bulk temperature to determine the average temperature polarization coefficient.

Recently, computational fluid dynamics (CFD) has been widely employed as a method for the simulation of fluid dynamic behavior in membrane modules. Ghadiri et al. [15] proposed a finite element method based on CFD for the simulation of DCMD, considering the heat and mass transfer in a flat-sheet module. Hasanizadeh et al. [16] and Rezakazemi [17] simulated the DCMD process for water diffusion across the membrane to produce water from saltwater under different conditions using a CFD approach. DCMD systems have been studied extensively by many authors assuming in most cases that convection can be ignored in comparison with diffusion in the mass transfer equation. However, the influence of the counter diffusion velocity on typical DCMD systems makes the convective term an efficient mass transfer mechanism.

To the best of the authors' knowledge, the impact of counter diffusion velocity on the flow rate of freshwater produced through the hydrophobic membranes used in DCMD has not been studied yet. To investigate the effect of counter diffusion velocity on the total distillate flux of DCMD systems, a comprehensive two-dimensional (2D) CFD simulation of DCMD based on the conservation equations of mass, momentum, and energy was conducted in this study. Raoult's law was applied to predict the vapor pressure at both membrane interfaces. The obtained results were validated by comparing the simulation results with the experimental results obtained by Hwang et al. [18]. The temperature distribution for all three layers and the velocity distribution for both the feed and permeate channels were determined. Another important objective of the present study was to investigate strategies for increasing the gain output ratio (GOR) and transmembrane flux. Hence, the effect of different parameters on GOR and transmembrane flux was investigated in this study. Furthermore, the effects of the linear velocity, which is the most effective parameter on the temperature polarization coefficient, were studied and are presented here. Finally, the sensitivity analysis performed in this study indicates how the uncertainty in the performance of an MD system can be apportioned to different input parameters.

2. Principles of the DCMD process

Among the different MD configurations, DCMD was selected for the present study because of its effectiveness in the removal of nonvolatile compounds. This type of distillation also produces a more stable distillate flux than the others [19]. In DCMD, the hydrophobic microporous membrane is in direct contact with the feed and permeate channels, as illustrated in Fig. 1. The temperature difference between the feed channel's bulk stream and the permeate channel's bulk stream creates the required vapor pressure difference. For continuous operations, the feed and permeate aqueous streams under different temperature conditions are circulated tangentially to the DCMD membrane. Under such temperature conditions, water molecules evaporate at the (hot) interface between the membrane and the feed

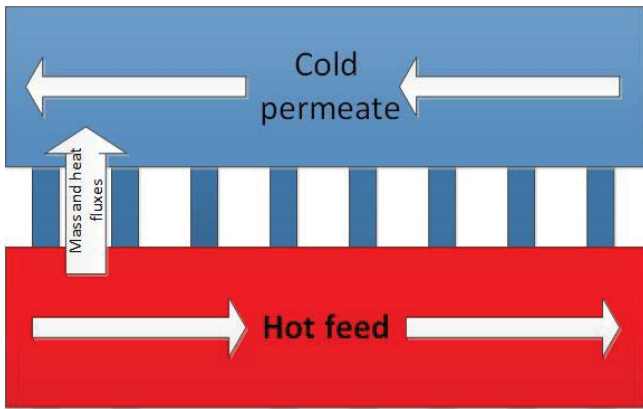


Fig. 1. Direct contact membrane distillation configuration.

channel. The vapor diffuses through the membrane pores and condenses at the (cold) interface placed between the membrane and the permeate channel.

The membrane used in MD systems acts as a physical barrier to sustain the liquid–vapor interfaces formed at the entrances of the membrane pores. Water vapor generated in the feed-membrane interface are transported across the membrane pores according to the vapor/liquid equilibrium principle, and both heat and mass transfer occur simultaneously through the membrane. MD membranes prepared by different techniques, such as sintering, stretching, phase inversion, and electrospinning, should exhibit a low membrane resistance to mass transfer and low thermal conductivity of the membrane material.

The hydrophobic nature of the membrane prevents liquid water (brine) from penetrating the feed channel to the membrane pores. The surface tension can maintain the liquid–vapor interface up to a certain pressure, beyond which liquid water penetrates the membrane pores. This pressure, called the liquid entry pressure (LEP), can be determined by different experimental tests and theoretically by the Young–Laplace equation as follows [12]:

$$LEP = \frac{-4\sigma\cos\theta}{d_p} \quad (1)$$

where σ , θ , and d_p are the surface tension of the liquid phase, the contact angle between the fluid and membrane, and average membrane pore diameter, respectively. In addition to the flow driven by the pressure difference, another mode of water transfer through the membrane is by phase change. In microporous and nanoporous materials, condensation of transmembrane vapor, known as capillary condensation, may occur at low relative humidity depending on the size and geometry of the pores. Uhlhorn et al. [20] proposed six different modes to demonstrate the possibility of capillary condensation for transmembrane gases in small pores. As observed in Fig. 2, in case of C1, there is no condensation in the pores when the capillary condensation pressure, calculated by Kelvin correlations introduced in Eq. (2), is higher than the partial pressures at both interfaces. In other cases, condensation occurred in the pores.

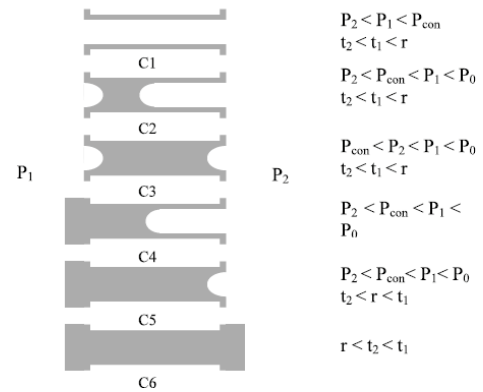


Fig. 2. Six modes of condensation in porous materials [21]. P_1 , P_2 , and P_{con} are the upstream pressure, downstream pressure, and capillary condensation pressure, respectively.

$$\ln \frac{P_{con}}{P_{sat}} = -\frac{2H\gamma V_l}{RT} \quad (2)$$

Here, P_{con} , P_{sat} , H , γ , V_l , R , and T refer to the capillary condensation pressure, saturation vapor pressure, mean curvature of the meniscus, liquid/vapor surface tension, liquid molar volume, ideal gas constant, and temperature, respectively. The mean curvature of the meniscus depends on the portion of the surface of a sphere created with radius r_s on the membrane material in the pores. The radius of the sphere (r_s) is a function of only the contact angle (θ); therefore, Eq. (2) is derived from the following expression:

$$\ln \frac{P_{con}}{P_{sat}} = -\frac{2\gamma\cos\theta V_l}{RT r_s} \quad (3)$$

For different porous materials, the possibility of condensation would be different, and it actually depends on the relative intensity of cohesiveness of water vapor molecules and adhesion between the water vapor molecules and membrane walls. These forces are responsible for the contact angle between the liquid surface and membrane wall. In the case of a non-wettable membrane or hydrophobic materials, the contact angle is more than 90° , which leads to the first mode for the MD process in Fig. 2 [21].

3. Model development

A mathematical model was developed in the present study to predict the important features of DCMD, including the distillate flux, temperature and velocity distributions, and GOR by considering the role of counter diffusion velocity in MD systems. A steady-state 2D model of a DCMD flat-sheet membrane module is constructed. To achieve more accuracy, the values of viscosity, density, specific heat at constant pressure, and thermal conductivity for the feed channel are considered as a function of temperature and salinity presented in the Engineering Equation Solver (EES) library [22,23]. In addition, to determine all the properties mentioned above for the permeate

channel, these are considered as a function of temperature. The algorithm of the numerical solution is depicted in Fig. 3.

For validation, the data reported by Hwang et al. [18] were used. The membrane properties used in this study and the applied experimental conditions [18] are listed in Table 1. Mass conservation in the membrane based on the transport of diluted species in porous media, heat balance including both convection and conduction in all layers, and momentum conservation for both feed and permeate channels are considered in the model.

To simplify the governing equations, which in turn lowers the costs of calculation, the model is developed using the following assumptions:

- Steady-state operation and laminar flow for the feed and permeate streams.
- Concentrated aggregation of NaCl (salt) in the solution is neglected.
- No chemical reaction occurs during the operation.
- Heat loss to the environment is neglected.
- Macroscopic membrane characteristics, such as mean pore diameter, are considered to calculate the Knudsen diffusion coefficient.

3.1. Conservation of momentum and energy in channels

Momentum conservation in the feed and permeate channels is considered assuming steady-state conditions as follows [10,15,18]:

$$-\nabla \cdot \mu (\nabla V + (\nabla V)^T) + V \cdot \nabla (\rho V) + \nabla P = \rho g \quad (4)$$

$$\nabla \cdot (\rho V) = 0$$

where μ (Pa s), V (m s⁻¹), P (Pa), ρ (kg m⁻³), and g (m s⁻²) refer to the dynamic viscosity, velocity field, pressure, density, and gravitational acceleration, respectively.

The energy balance equation including convection and conduction for both feed and permeate flows in the feed channel is as follows [24,25]:

$$\nabla \cdot (K \nabla T) + S_h = \rho C_p (V \cdot \nabla T) \quad (5)$$

Here, C_p (J/kg K⁻¹), T (K), and K (W m K⁻¹) are the specific heat capacity at constant pressure, temperature field, and thermal conductivity, respectively. In addition, S_h (W m⁻²) is the energy source term produced by evaporation at the feed membrane interface and released by condensation at the permeate membrane interface. Hence, the velocity and temperature distributions are determined by solving the above equation for both the feed and permeate channels. As previously mentioned, to achieve more accurate results, the values of viscosity, density, specific heat at constant pressure, and thermal conductivity for the feed channel are considered as functions of temperature and salinity presented in the EES library, whereas these parameters for the pure water flow in the permeate channel are determined as a function of temperature.

3.2. Transport through the membrane

Conjugated heat and mass transfer occur through the membrane layer. The transport mechanism of volatile molecules through the membrane pores is complex and depends on different factors such as the total pressure difference and Knudsen number. In general, three different modes of mass transfer through the membrane are considered: (1) convective flow, which arises through the large pores when a total pressure difference across the pore exists, (2) ordinary molecular diffusion, where the water molecules diffuse via the air trapped inside the larger pores of the membrane, and (3) Knudsen diffusion in the nanopores where the characteristic length is comparable to or smaller than the mean free path of water molecules at a given

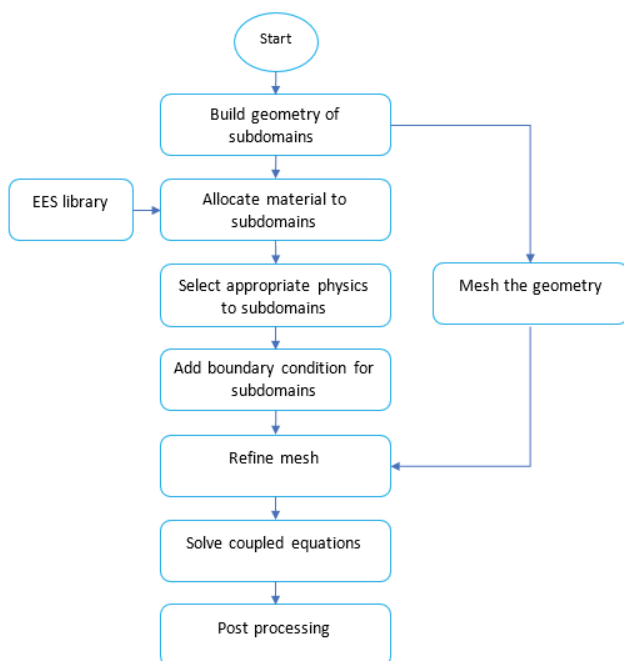


Fig. 3. Flowchart of the procedure for numerical solution.

Table 1
Design parameters for the numerical simulation and experimental conditions [16]

Parameters	Value
Inlet temperature in feed channel, K	333
Inlet temperature in permeate channel, K	293
NaCl mass fraction, %	1%
Membrane material	PTFE
Nominal pore size, μm	0.22
Membrane thickness, μm	100
Porosity	0.83
Module width, m	0.15
Module length, m	0.4
Hot channel height, m	0.001
Cold channel height, m	0.001
Velocity of feed and permeate flows, m s ⁻¹	0.5

pressure and temperature [19]. Knudsen diffusion and ordinary molecular diffusion model the effects of collisions with structural boundaries and intermolecular collisions, respectively [26]. The Knudsen number is defined as follows:

$$Kn = \frac{\lambda}{d_p} \quad (6)$$

where λ is the mean free path of water molecules and d_p is the characteristic pore diameter of the membrane. The mean free path of water molecules in the vapor phase can be determined using the following Boltzmann equation [13,26]:

$$\lambda = \frac{K_B T}{\sqrt{2} P_m \sigma_w^2} \quad (7)$$

where K_B , T , P_m , and σ_w are the Boltzmann constant, temperature, mean pressure within membrane pores, and collision diameter of water molecules, which is equal to 2.611×10^{-4} μm . At atmospheric pressure and for the typical pore diameters of membranes frequently used in MD (between 10 nm and 1 μm), the Knudsen number falls in the range $0.1 < Kn < 10$; therefore, superposition of both molecular diffusion and Knudsen diffusion is expected. For typical DCMD systems where no deaeration is performed, there is no total pressure difference between both sides of the membrane because the module is usually open to the ambient; thus, the contribution of mass transfer driven by pressure difference is negligible. Hence, the dominant mode of mass transfer through the membrane is diffusion, including Knudsen diffusion and ordinary molecular diffusion.

Under the aforementioned conditions, a binary mixture of gas containing water vapor and the air is present in the pore volume of the membrane. For transmembrane water vapor transport, the structural properties of the membrane, and the presence of air in the membrane pore volume introduce mass transfer resistances. Presumably, a liquid stream would carry a certain amount of dissolved air to the membrane interface, where there is phase equilibrium with the gas mixture containing water vapor and air. If the dissolved air concentration in the liquid stream changes, the equilibrium changes, and air would enter the membrane or be removed from it. However, in an equilibrium state, air is assumed to be constant, akin to a stagnant film, owing to the low flux. The result is a binary mixture of water vapor and air in the membrane, and the air acts as a stagnant gas that is trapped in the pores of the membrane and there is no net flux of air into the membrane. To satisfy a zero net flux condition of air, a counter diffusion velocity must be considered [27].

It has been assumed in most previous studies that the convection term can be neglected in the continuity equation for the DCMD process; however, the influence of the counter diffusion velocity would make the convective term significant. Consider the mass conservation equation for the membrane layer as follows:

$$\nabla \cdot (D_m \nabla C_{m,w}) = u (\nabla \cdot C_{m,w}) \quad (8)$$

where $C_{m,w}$ and D_m are the water concentration in the membrane and the water diffusion coefficient within the membrane, respectively. The diffusion coefficient is obtained as follows based on Knudsen and ordinary molecular diffusion [13,17,28]:

$$D_m = \left[\left(\frac{1}{D_{Kn}} + \frac{1}{D_{OM}} \right)^{-1} \right] \quad (9)$$

where D_{Kn} and D_{OM} refer to Knudsen diffusion and ordinary molecular diffusion coefficients, respectively. The ordinary molecular diffusion coefficient represents the effect of intermolecular collisions, which can be determined using different expressions [29,30]. The Knudsen diffusion coefficient captures the influence of molecular collisions with the structural boundaries and can be calculated as follows [15,27,31]:

$$D_{Kn} = \left[\frac{d_p}{3} \left(\frac{8RT}{\pi M} \right)^{0.5} \right] \quad (10)$$

where D_{Kn} ($\text{m}^2 \text{s}^{-1}$), d_p (m), T (K), and M (kg mol^{-1}) are the Knudsen diffusion coefficient of water in the membrane, and the characteristic pore diameter, temperature, and molecular weight of water, respectively.

The energy balance in the membrane, which considers the heat transfer through the membrane pores and solid, is as follows:

$$\nabla \cdot (K_m \nabla T_m) + S_h = \rho_m C_{pm} (V \cdot \nabla T_m) \quad (11)$$

Here, C_{pm} (J kg K^{-1}), T_m (K), K_m (W m K^{-1}), and S_h (W m^{-2}) are the specific heat capacity at constant pressure, temperature field of the membrane, thermal conductivity of the membrane, and energy source term, respectively. The membrane thermal conductivity can be determined as a weighted average (based on volume) of the membrane thermal conductivities of the corresponding solid and vapor phases as follows [32]:

$$K_m = \varepsilon K_{v,p} + (1 - \varepsilon) K_s \quad (12)$$

where $K_{v,p}$ and K_s represent the thermal conductivity of the vapor and solid membrane, respectively, and ε is the porosity of the membrane.

As previously mentioned, the effect of counter diffusion velocity is not negligible, and thus the term of convection in the continuity equation plays an important role. Because air is assumed to be absolutely stagnant in the membrane, the net air flux would be zero [27].

$$n_a = \rho_a V_{CD} + J_a = 0 \quad (13)$$

To satisfy Eq. (13), the velocity must be equal to the ratio of the air diffusional flux to the air density. This velocity is called the counter diffusion velocity and is defined as follows:

$$V_{CD} = \frac{-J_a}{\rho_a} = \frac{J_w}{\rho_a} \quad (14)$$

where n_a , J_a , ρ_a , and V_{CD} are the net air flux, air diffusional flux, air density, and counter diffusion velocity, respectively.

3.3. Computational domain and boundary conditions

Fig. 4 shows the computational domain constructed for the 2D model of the present study. After the mesh independence test, an adaptive independent mesh refinement, which generates the best and minimal meshes, was chosen to mesh the DCMD geometry. A scaling factor of 100 was applied in the y -direction because of the large difference between x and y . Design dimensions that show the height of the hot channel, cold channel, and membrane, along with the module width, are specified in Table 1.

The boundary conditions of momentum and energy transport for the feed and permeate channels are as follows:

at $x = 0$

$$V_f = V_{f,i}, T_f = T_{f,i}$$

at $x = L$

$$P_f = P_{atm} \text{ (outlet boundary)}, -n \cdot q = 0 \text{ (convective flux)}$$

at $y = 0$

$$V_f = 0 \text{ (no slip wall)}, \frac{\partial T_f}{\partial y} = 0 \text{ (isothermal)}$$

at $y = a$

$$V_f = 0 \text{ (no slip wall)}, \\ S_h = -J \times h_{ig} \text{ (energy source term (heat flux) produced by evaporation)}$$

at $x = 0$

$$P_p = P_{atm} \text{ (outlet boundary)}, -n \cdot q = 0 \text{ (convective flux)}$$

at $x = L$

$$V_p = V_{p,i}, T_p = T_{p,i}$$

at $y = b$

$$V_p = 0 \text{ (no slip wall)}, T_p = T_m$$

at $y = c$

$$V_p = 0 \text{ (no slip wall)}, \frac{\partial T_p}{\partial y} = 0 \text{ (isothermal)}$$

where $V_{f,i}$, $T_{f,i}$, $T_{m,i}$, and P_{atm} are the inlet feed velocity, inlet feed temperature, feed-membrane interface temperature, and atmospheric pressure, respectively. In addition, $V_{p,i}$ and

$T_{p,i}$ refer to the inlet permeate velocity and inlet permeate temperature, respectively. The amount of inlet velocities and temperatures, along with other design parameters, are already mentioned in Table 1. In addition, S_h refers to the heat flux produced or released at membrane interfaces. The value of S_h is dependent on the total distillate flux and latent heat.

The boundary conditions for the mass transfer and energy balance equations in the membrane domain are as follows:

at $x = 0$

$$\frac{\partial C_m}{\partial x} = 0 \text{ (no flux)}, \frac{\partial T_m}{\partial x} = 0 \text{ (isothermal)}$$

at $x = L$

$$\frac{\partial C_m}{\partial x} = 0 \text{ (no flux)}, \frac{\partial T_m}{\partial x} = 0 \text{ (isothermal)}$$

at $y = a$

$$C_{m,w} = C_h \text{ (using Raoult's law and Antoine's equation)}, \\ T_m = T_f$$

at $y = b$

$$C_{m,w} = C_c \text{ (using Raoult's law and Antoine's equation)}, \\ S_h = J \times h_{ig} \text{ (Energy source term (heat flux) released by condensation)}$$

As mentioned above, the water vapor concentration and water vapor mass or mole fraction at both membrane interfaces can be determined by assuming Raoult's law and ideal gas behavior for the water vapor flow. According to Raoult's law, the water vapor partial pressure at both interfaces for the dominant species in the liquid phase is approximately equal to the saturated pressure at the local temperature [33,34]. To determine the air partial pressure at the liquid-vapor interface, Henry's law was applied. The Antoine equation can be used to calculate the saturated pressure at the local temperature.

4. Results and discussion

This section consists of three parts: validation of the baseline case, parametric study, and performance evaluation

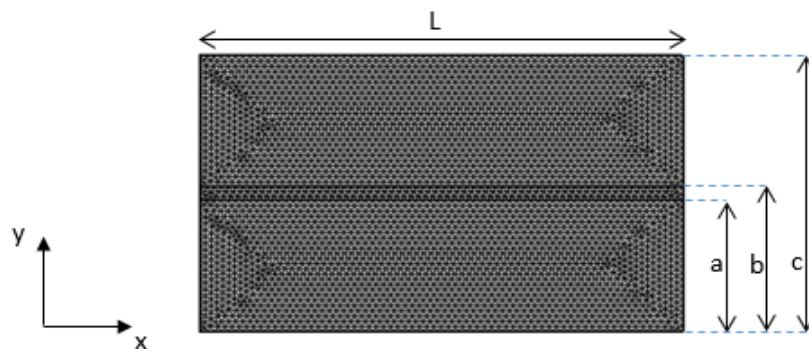


Fig. 4. 2D meshed computational domain constructed using COMSOL multiphysics software.

of the selected DCMD, and uncertainty and global sensitivity analysis.

4.1. Validation of baseline case

In this section, the results obtained from the present model considering the counter diffusion velocity are compared with the experimental data of an actual system and the predicted responses of the Hwang et al. [18] model. The experimental conditions and module specifications, including the module dimensions and membrane properties used in this study, are listed in Table 1. An aqueous solution containing 1% NaCl and water flows to the feed channel with feed inlet temperature and velocity of 333 K and 0.5 m s⁻¹, respectively, while permeate water enters simultaneously to the permeate channel at 293 K and 0.5 m s⁻¹. Table 2 lists the experimental and simulation results obtained by Hwang et al. [18] and the present model for feed and permeate outlet temperatures. As presented in Table 2, there is good agreement between the predicted responses of the present model and experimental data. In addition, the modeling errors for both the present model and the Hwang et al. [18] model are compared in Table 2.

For the feed and permeate outlet temperatures, maximum deviations of 0.26% and 0.53% were observed between the model and experimental data when the velocities of both feed and permeate flows are 0.50 m s⁻¹. Hence, the present model results show better agreement with the experimental results in comparison with those presented by Hwang et al. [18]. This confirms that by considering the counter diffusion velocity, the 2D DCMD model developed in this study is accurate in predicting the DCMD operation.

Fig. 5 illustrates the temperature distribution along the channel of the module obtained for the present computational domain and under the aforementioned conditions for the present model and experimental data. As observed in this Fig. 5, good correspondence exists between them.

4.2. Parametric study and performance evaluation of selected DCMD

Fig. 6 shows the temperature distribution of the entire domain. Because the driving force in the DCMD is the partial pressure gradient of the water across the membrane, the temperature distribution in the DCMD is of great importance for the modeling of DCMD systems. It is noted that porous media and porosity significantly affect the

thermal conductivity, which can be determined by Eq. (12), and the thermal conductivity of the commercial membrane used for the present simulation is 0.25 J(m K)⁻¹, as specified by the manufacturer.

Fig. 7a depicts the values for the water vapor partial pressure on both sides of the membrane. The temperatures at the membrane interfaces shown in Fig. 6 were converted to vapor partial pressures using the Antoine equation. As observed in Fig. 7a, the water vapor partial pressure difference decreases downstream of the feed channel. The partial pressure difference at the beginning of the module is approximately 11 kPa, and it reduces to approximately 6 kPa at the end of the module. Moreover, the decrease in vapor pressure for the feed–membrane interface was greater than that for the permeate–membrane interface because of the exponential nature of the Antoine equation and temperature of the interfaces. Fig. 7b depicts the amount of total transmembrane flux and counter diffusion transmembrane flux of the produced fresh water at the interface of the membrane and permeate channel.

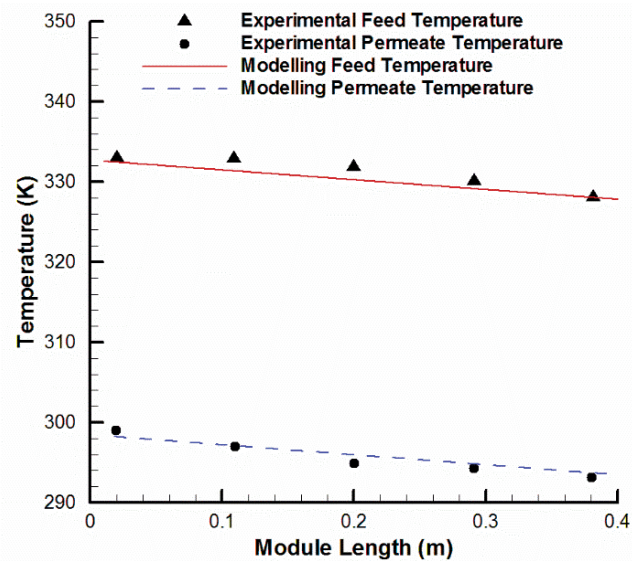


Fig. 5. Temperature distribution along the channel; feed inlet temperature = 333 K; permeate inlet temperature = 293 K; NaCl concentration = 1%; linear velocity of 0.50 m s⁻¹ in both feed and permeate channels.

Table 2

Comparison of relative errors of outlet temperatures for experimental and predicted responses by Hwang et al. [18] and present models

V	Feed outlet temperature (K)					Permeate outlet temperature (K)				
	Exp. data [18]	Hwang model [18]	Err. (%)	Present model	Err. (%)	Exp. data [18]	Hwang model [18]	Err. (%)	Present model	Err. (%)
0.17	323.25	322.65	0.19	322.39	0.26	302.25	303.65	0.5	303.87	0.53
0.28	325.45	325.85	0.12	325.04	0.12	300.55	300.65	0.03	301.28	0.07
0.39	327.05	327.45	0.12	326.76	0.09	299.45	298.85	0.2	299.53	0.03
0.50	328.25	328.45	0.07	327.81	0.13	298.95	297.85	0.37	298.46	0.16

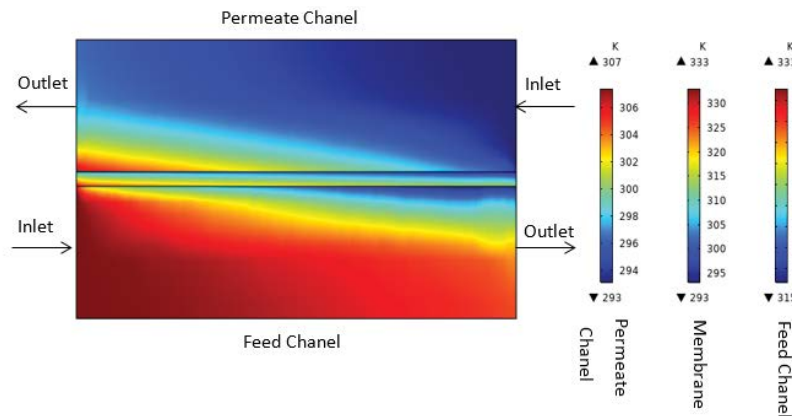


Fig. 6. Temperature distribution in DCMD; left, middle, and right legends show the temperature range of permeate, membrane, and feed, respectively.

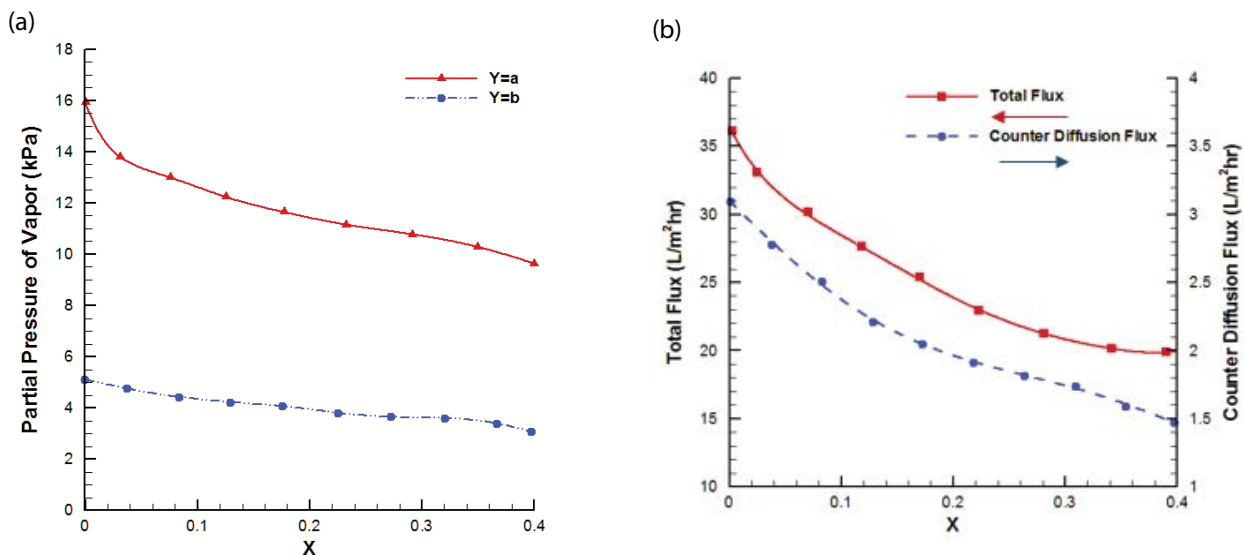


Fig. 7. (a) Partial pressure of water vapor along the channel and (b) total flux and counter diffusion flux of condensed fresh water at the interface of membrane and permeate channel (feed inlet temperature = 333 K; permeate inlet temperature = 293 K; feed and permeate velocity = 0.5 m s⁻¹; NaCl mass fraction = 1%).

Fig. 8 shows the effect of linear velocity on the transmembrane flux of condensed water obtained by the Hwang et al. [18] model and experimental data in comparison with the flux obtained by the present model. It is worth mentioning that the concept of linear velocity is, in fact, the constant inlet velocity in each channel. As illustrated, properly implementing the counter diffusion velocity in the computation of the total flux improves the accuracy of prediction, in comparison with that obtained by Hwang et al. [18]. The main reason for such improvement is the fact that the counter diffusion velocity causes the convective term to be effective in computing the total flux. Considering mass transport through membrane pores due to diffusion alone might cause modeling errors, especially at higher linear velocities, because the counter diffusion flux increases with an increase in velocity. Including the counter diffusion velocity in evaluating the net flux leads

to a decrease in the average error between the experimental data and simulation results from 10.5% indicated by previous studies to 2% calculated in the present study.

The GOR or thermal efficiency is the ratio of the amount of latent heat required to evaporate liquid water over the total heat transferred through the membrane, that is:

$$GOR = \frac{Q_i}{Q_i + Q_c} \tag{15}$$

where Q_i and Q_c are the required heat transfer rate for evaporation and heat transfer rate by conduction, respectively. Fig. 9 shows the effect of the feed inlet temperature on the total transmembrane flux, counter diffusion transmembrane flux, and GOR at a constant permeate inlet temperature. As shown in Fig. 9, an exponential

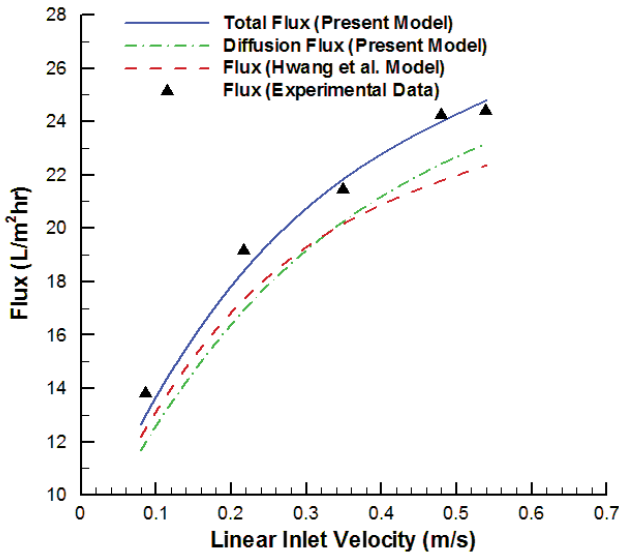


Fig. 8. Effect of linear velocity on transmembrane flux (feed inlet temperature of 333 K; permeate inlet temperature of 293 K; NaCl mass fraction of 1%).

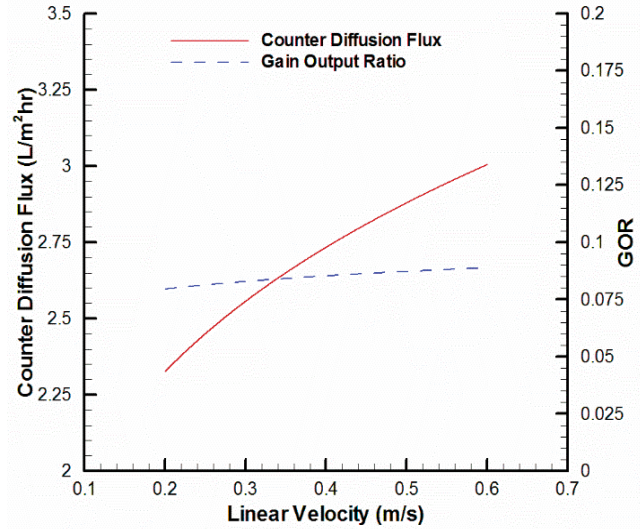


Fig. 10. Effect of linear velocity on counter diffusion flux and gain output ratio (feed inlet temperature = 333 K; permeate inlet temperature = 293 K; NaCl mass fraction = 1%).

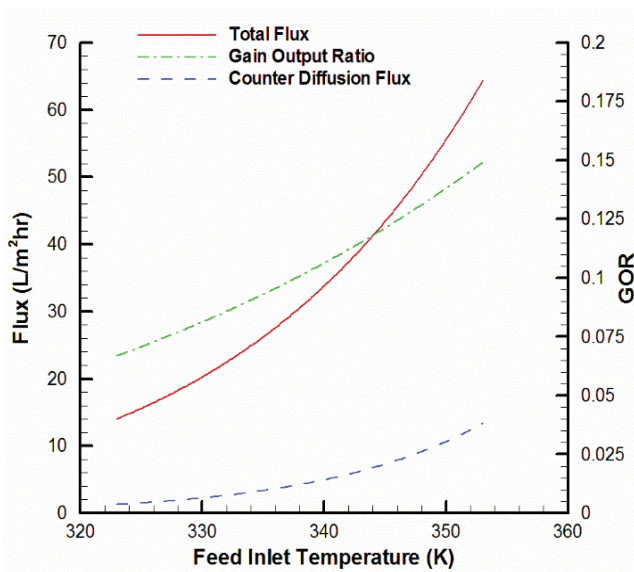


Fig. 9. Effect of feed inlet temperature on total and counter diffusion flux and gain output ratio (linear velocity at both feed and permeate sides of 0.50 m s⁻¹; permeate inlet temperature of 293 K; NaCl mass fraction of 1%).

enhancement in the total distillate flux can be observed with increasing feed inlet temperature, which increases the vapor pressure. In addition, the GOR increases approximately linearly with increasing feed inlet temperature.

The effect of linear velocity on GOR as an effective and sensitive parameter, together with the feed inlet temperature, is shown in Fig. 10. As depicted in Fig. 10, the GOR is not sensitive to the linear velocity of the feed and permeate flows. Meanwhile, the counter diffusion flux increases with linear velocity, as expected.

Fig. 11 shows the temperature variations along with the module height at the middle of the module length. Temperature polarization refers to a region of decreased temperature in comparison with the bulk temperature adjacent to the membrane interfaces in DCMD. This phenomenon occurs at both sides of the membrane in DCMD and introduces the heat transfer resistance, which causes a reduction in the effective temperature gradient and a corresponding reduction in the water partial pressure gradient in DCMD.

The strength of the temperature polarization is measured by a dimensionless parameter called the temperature polarization coefficient [24,33], which is defined as:

$$TPC = \frac{T_{fm} - T_{pm}}{T_{fb} - T_{pb}} \quad (16)$$

TPC is unity in an ideal case. Generally, if TPC is lower than 0.2, the DCMD process is limited by heat transfer, and the system design is considered poor. If TPC is greater than 0.6, mass transfer is more dominant than heat transfer. Two important parameters affecting the temperature polarization and its thickness boundary layer are the feed and permeate linear velocities. Under turbulent conditions, the thickness of the temperature polarization layer is reduced, leading to better maintenance of the driving force [24,28].

Fig. 12 shows the temperature polarization coefficient (Eq. (16)) vs. the linear velocity. One way to reduce temperature polarization is to increase the feed and permeate velocities. When the feed and permeate velocities increase, both the Reynolds and Nusselt numbers increase, and as a result, heat transfer of the feed and permeate channels is enhanced. Enhanced heat transfer brings the bulk temperature of the feed and permeate closer to the temperature at

the membrane interface. However, the flow rate or velocity must be varied with precautions not only to avoid membrane pore wetting, as the transmembrane hydrostatic pressure must be lower than the LEP (Eq. (1)), but also to assure working under high velocity to obtain high productivity. As illustrated in Fig. 12, the linear velocity is considered in the range of 0.1 and 0.7 m s⁻¹ for the numerical study on temperature polarization coefficient. Fig. 12 implies that for linear inlet velocities less than 0.2, the DCMD process is heat transfer limited and the DCMD module design is

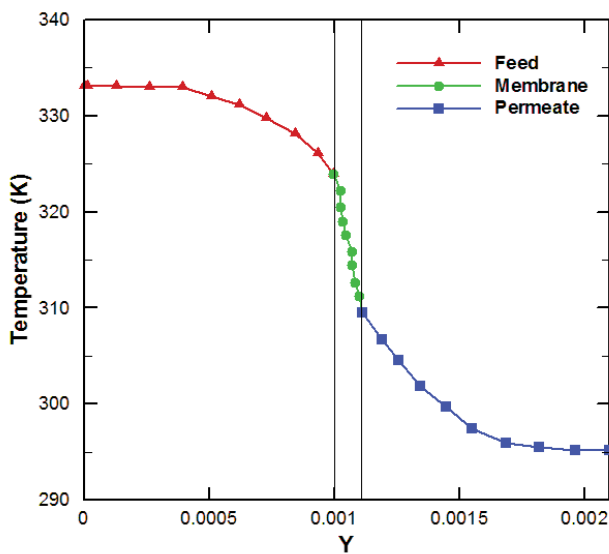


Fig. 11. Temperature profile along *y*-direction (module height) at the middle of module length (*x* = 0.2 m) (feed inlet temperature of 333 K; permeate inlet temperature of 293 K; feed and permeate velocity of 0.5 m s⁻¹; NaCl mass fraction of 1%).

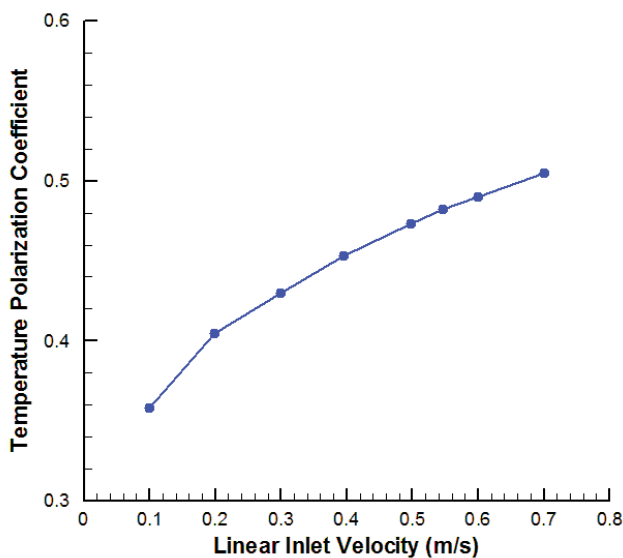


Fig. 12. Effect of linear velocity on temperature polarization coefficient (feed inlet temperature of 333 K; permeate inlet temperature of 293 K; NaCl concentration of 1%).

poor. Although, the DCMD process for linear inlet velocities more than 0.6 m s⁻¹ is mass transfer limited, the transmembrane hydrostatic pressure exceeds LEP.

The effect of the NaCl mass fraction on the transmembrane flux was studied. This task is accomplished for three different NaCl mass fractions of feed water by fixing the other parameters mentioned in Table 1, and the results are shown in Fig. 13. The transmembrane flux decreased by approximately 17.8%, from 24.1 to 19.8 L m² h⁻¹, when the NaCl concentration increased from 1 to 10 wt.%.

4.3. Uncertainty and global sensitivity analysis

Sensitivity analysis is the study of how uncertainty in the output of a mathematical model or system (numerical or otherwise) might be attributed to different input parameters [2]. A common practice in uncertainty analysis is uncertainty quantification and its propagation [33]. In the present work, a global sensitivity analysis technique is used to evaluate the effect of input parameters, including membrane thickness, feed inlet temperature, and feed linear velocity, on the output objectives, while all other input parameters are also varied based on their assigned distributions. The studied output objectives are the GOR, produced freshwater flow rate, and temperature polarization coefficient.

In this study, the partial derivatives of all input parameters are first calculated. Considering the partial derivatives and simulation range of each input parameter, the first-order sensitivity index of each input parameter affecting the output objectives can be determined. Indeed, sensitivity indices are quantitative measures of sensitivity. The main effect of the input parameter on the output variance is defined by the first-order sensitivity index as follows:

$$S_i = \frac{V_{x_i}(E_{x_i}(Y))}{V(Y)} \tag{17}$$

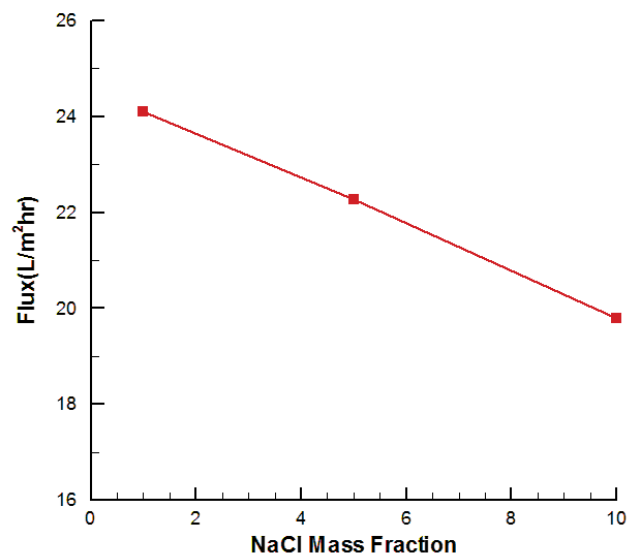


Fig. 13. Effect of NaCl mass fraction on transmembrane flux (feed inlet temperature = 333 K; permeate inlet temperature = 293 K; feed and permeate velocity = 0.5 m s⁻¹).

Table 3
Effect of different operation conditions on GOR and TPC

	Simulation range	GOR			TPC		
		Partial derivative	Sensitivity index	Effect	Partial derivative	Sensitivity index	Effect
δ	1–200 μm	–837.8	0.659	↓	2,331	0.886	↑
T_{fi}	310–350 K	0.0046	0.241	↑	–0.003	0.0912	↓
V_{fi}	0.25–0.75 m s^{-1}	0.0015	0.1	↑	0.052	0.0228	↑

where S_p , $V_x(E_x(Y))$, and $V(Y)$ are the sensitivity index, conditional variance, and unconditional variance, respectively. The sensitivity indices are positive numbers between 0 and 1. A higher sensitivity index represents a greater influence of the corresponding parameter on the output [35,36].

As observed in Figs. 9 and 10, increasing both the feed inlet temperature and the feed linear velocity enhances the GOR. The study of uncertainty in the GOR can be performed by the sensitivity analysis method described above.

Table 3 presents the effects of different parameters on GOR and TPC. The results indicate that although the membrane thickness has the strongest positive influence on TPC, it shows a negative effect on GOR. It is concluded that the mass transfer imposed by the membrane is the dominant resistance in this process and no significant heat transfer improvement is needed in the current membrane contactor. As illustrated in Fig. 9, increasing the feed inlet temperature enhances the GOR corresponding to an increase in the driving force, which is a partial pressure difference. Additionally, increasing the feed inlet temperature leads to some heat loss in the feed region, which results in TPC reduction.

The feed linear velocity plays a positive role in both GOR and TPC. This can be due to the heat transfer coefficient increment, which is imposed by the velocity increment in the mentioned regions.

5. Conclusion

A two-dimensional mathematical model was developed to predict the effects of the counter diffusion velocity on the total flux of the DCMD process. In the present study, a counter-current flat-sheet membrane contactor used for direct-contact membrane distillation was modeled and investigated. The counter diffusion velocity on the DCMD was found to reduce the average error between the experimental total flux and the simulation total flux from 10.5% found in previous studies [18] to 2% calculated in the present study. Furthermore, the present results indicate that an increase in the feed inlet temperature significantly increases the total distillate flux. It was also found that a higher linear inlet velocity reduces the negative effect of temperature polarization as a heat transfer resistance. However, the flow rate and velocity must be varied with due precautions to avoid membrane pore wetting and assure operation under high velocity. It is noted that an increase in both the feed inlet temperature and linear velocity enhances the GOR. Moreover, the model results show that the flux decreased with an increase in the NaCl mass fraction because of the reduction in pressure gradient as the driving force and polarization formed on the membrane interface. A

sensitivity analysis of some effective parameters on the GOR and temperature polarization coefficient was performed. The analysis reveals that the membrane thickness has the strongest influence on GOR and TPC in comparison with the feed inlet temperature and feed linear velocity. The feed inlet temperature is a more influential design parameter than the feed linear velocity in this system.

Acknowledgments

This work was supported by the National Natural Science Foundation of China (No. 21776226) and the China Scholarship Council (2017SLJ020343, 2019SLJ017820). PCS acknowledges financial support from the Hubei-100 Plan of China.

Symbols

C_p	–	Specific heat capacity at constant pressure, $\text{J kg}^{-1} \text{K}^{-1}$
K	–	Thermal conductivity, $\text{W m}^{-1} \text{K}^{-1}$
T	–	Temperature, K
T_m	–	Membrane temperature, K
Kn	–	Knudsen number, –
K_B	–	Boltzmann constant, J K^{-1}
P	–	Pressure, Pa
D^m	–	Diffusion coefficient, $\text{m}^2 \text{s}^{-1}$
D_{Kn}^m	–	Knudsen diffusion coefficient, $\text{m}^2 \text{s}^{-1}$
D_{OM}	–	Ordinary molecular diffusion coefficient, $\text{m}^2 \text{s}^{-1}$
M	–	Molecular weight, kg mol^{-1}
K_m	–	Membrane effective thermal conductivity, $\text{W m}^{-1} \text{K}^{-1}$
K_s	–	Solid thermal conductivity, $\text{W m}^{-1} \text{K}^{-1}$
$K_{v,p}$	–	Vapor thermal conductivity, $\text{W m}^{-1} \text{K}^{-1}$
J_a	–	Air diffusional flux, $\text{kg m}^{-2} \text{s}^{-1}$
n_a	–	Air total flux, $\text{kg m}^{-2} \text{s}^{-1}$
Q_l	–	Heat transfer rate for evaporation, J
Q_c	–	Conductive heat transfer rate, J
T_{im}	–	Feed-membrane interface temperature, K
T_{pm}	–	Permeate-membrane interface temperature, K
T_{fb}	–	Feed bulk temperature, K
T_{pb}	–	Permeate Bulk temperature, K
d_p	–	Pore diameter, m
\dot{V}	–	Velocity, m s^{-1}
g	–	Gravity acceleration, m s^{-2}
r_s	–	Sphere radius, m
H	–	Mean curvature of the meniscus, m^{-1}
V_l	–	Liquid molar volume, $\text{m}^3 \text{mol}^{-1}$
\dot{V}_{CD}	–	Counter diffusion velocity, m s^{-1}
S_h	–	Energy source term (heat flux), W m^{-2}

Greek

σ_w	—	Collision diameter, m
σ	—	Surface tension, J m ⁻²
λ	—	Mean free path, m
μ	—	Dynamic viscosity, Pa s
ρ	—	Density, kg m ⁻³
ρ_a	—	Air density, kg m ⁻³

References

- [1] H.T. El-Dessouky, H.M. Ettouney, *Fundamentals of Salt Water Desalination*, Elsevier, Amsterdam, 2002.
- [2] H. Bazargan Harandi, M. Rahnama, E. Jahanshahi Javaran, A. Asadi, Performance optimization of a multi stage flash desalination unit with thermal vapor compression using genetic algorithm, *Appl. Thermal Eng.*, 123 (2017) 1106–1119.
- [3] D. Wu, A. Gao, H. Zhao, X. Feng, Pervaporative desalination of high-salinity water, *Chem. Eng. Res. Des.*, 136 (2018) 154–164.
- [4] G. Gopi, G. Arthanareeswaran, A. Ismail, Perspective of renewable desalination by using membrane distillation, *Chem. Eng. Res. Des.*, 144 (2019) 520–537.
- [5] P. Biniaz, N. Torabi Ardekani, M.A. Makarem, M.R. Rahimpour, Water and wastewater treatment systems by novel integrated membrane distillation (MD), *ChemEngineering*, 3 (2019) 8, doi: 10.3390/chemengineering3010008.
- [6] D. Winter, J. Koschikowski, S. Ripperger, Desalination using membrane distillation: flux enhancement by feed water deaeration on spiral-wound modules, *J. Membr. Sci.*, 423 (2012) 215–224.
- [7] D. González, J. Amigo, F. Suárez, Membrane distillation: perspectives for sustainable and improved desalination, *Renewable Sustainable Energy Rev.*, 80 (2017) 238–259.
- [8] K.W. Lawson, D.R. Lloyd, Membrane distillation, *J. Membr. Sci.*, 124 (1997) 1–25.
- [9] R. Schofield, A. Fane, C. Fell, Heat and mass transfer in membrane distillation, *J. Membr. Sci.*, 33 (1987) 299–313.
- [10] M. Khayet, T. Matsuura, J. Mengual, Porous hydrophobic/hydrophilic composite membranes: estimation of the hydrophobic-layer thickness, *J. Membr. Sci.*, 266 (2005) 68–79.
- [11] Ó. Andrésdóttir, C.L. Ong, M. Nabavi, S. Paredes, A.S.G. Khalil, B. Michel, D. Poulikakos, An experimentally optimized model for heat and mass transfer in direct contact membrane distillation, *Int. J. Heat Mass Transfer*, 66 (2013) 855–867.
- [12] D. Winter, Membrane Distillation - a Thermodynamic, Technological and Economic Analysis, Doctoral Dissertation, Department of Mechanical and Process Engineering, University of Kaiserslautern, Germany, 2014.
- [13] M. Khayet, T. Matsuura, *Membrane Distillation: Principles and Applications*. 2011: Elsevier.
- [14] Y.M. Manawi, M.A.M.M. Khraisheh, A.K. Fard, F. Benyahia, S. Adham, A predictive model for the assessment of the temperature polarization effect in direct contact membrane distillation desalination of high salinity feed, *Desalination*, 341 (2014) 38–49.
- [15] M. Ghadiri, S. Fakhri, S. Shirazian, Modeling and CFD simulation of water desalination using nanoporous membrane contactors, *Ind. Eng. Chem. Res.*, 52 (2013) 3490–3498.
- [16] M. Hasanizadeh, P. Jafari, B. Farshighazani, M.K. Moraveji, CFD simulation of heat and mass transport for water transfer through hydrophilic membrane in direct-contact membrane distillation process, *Desal. Water Treat.*, 57 (2016) 18109–18119.
- [17] M. Rezakazemi, CFD simulation of seawater purification using direct contact membrane desalination (DCMD) system, *Desalination*, 443 (2018) 323–332.
- [18] H.J. Hwang, K. He, S. Gray, J. Zhang, I.S. Moon, Direct contact membrane distillation (DCMD): experimental study on the commercial PTFE membrane and modeling, *J. Membr. Sci.*, 371 (2011) 90–98.
- [19] M.M.A. Shirazi, A. Kargari, A.F. Ismail, T. Matsuura, Computational fluid dynamic (CFD) opportunities applied to the membrane distillation process: state-of-the-art and perspectives, *Desalination*, 377 (2016) 73–90.
- [20] R. Uhlhorn, K. Keizer, A. Burggraaf, Gas transport and separation with ceramic membranes. Part I. Multilayer diffusion and capillary condensation, *J. Membr. Sci.*, 66 (1992) 259–269.
- [21] P. Uchytil, R. Petrickovic, S. Thomas, A. Seidel-Morgenstern, Influence of capillary condensation effects on mass transport through porous membranes, *Sep. Purif. Technol.*, 33 (2003) 273–281.
- [22] D. Jamieson, J. Tudhope, R. Morris, G. Cartwright, Physical properties of sea water solutions: heat capacity, *Desalination*, 7 (1969) 23–30.
- [23] M.H. Sharqawy, J.H. Lienhard, S.M. Zubair, Thermophysical properties of seawater: a review of existing correlations and data, *Desal. Water Treat.*, 16 (2010) 354–380.
- [24] Z. Kuang, R. Long, Z. Liu, W. Liu, Analysis of temperature and concentration polarizations for performance improvement in direct contact membrane distillation, *Int. J. Heat Mass Transfer*, 145 (2019), doi: 10.1016/j.ijheatmasstransfer.2019.118724.
- [25] P. Yazgan-Birgi, M.I.H. Ali, H.A. Arafat, Comparative performance assessment of flat sheet and hollow fiber DCMD processes using CFD modeling, *Sep. Purif. Technol.*, 212 (2019) 709–722.
- [26] R.H. Perry, *Chemical Engineers' Handbook*, Mcgraw-Hill Book, New York, NY, 1954.
- [27] E.L. Cussler, E.L. Cussler, *Diffusion: Mass Transfer in Fluid Systems*, Cambridge University Press, Cambridge, 2009.
- [28] R.A. Johnson, M.H. Nguyen, *Understanding Membrane Distillation and Osmotic Distillation*, John Wiley & Sons, Inc., 111 River Street, Hoboken, NJ 07030, USA, 2017.
- [29] H. Chiang, P. Chiang, Y. Chiang, E. Chang, Diffusivity of microporous carbon for benzene and methyl-ethyl ketone adsorption, *Chemosphere*, 38 (1999) 2733–2746.
- [30] J. Xu, R. Li, L. Wang, J. Li, X. Sun, Removal of benzene from nitrogen by using polypropylene hollow fiber gas-liquid membrane contactor, *Sep. Purif. Technol.*, 68 (2009) 75–82.
- [31] W.M. Deen, *Analysis of Transport Phenomena*, Oxford University Press, New York, NY, 1998.
- [32] A. Deshmukh, J. Lee, Membrane desalination performance governed by molecular reflection at the liquid-vapor interface, *Int. J. Heat Mass Transfer*, 140 (2019) 1006–1022.
- [33] H. Hayer, O. Bakhtiari, T. Mohammadi, Simulation of momentum, heat and mass transfer in direct contact membrane distillation: a computational fluid dynamics approach, *J. Ind. Eng. Chem.*, 21 (2015) 1379–1382.
- [34] J.H. Lienhard, *A Heat Transfer Textbook*, Phlogiston Press, Cambridge, Massachusetts, USA, 2019.
- [35] R. Haghbakhsh, H. Hayer, M. Saidi, S. Keshtkari, F. Esmail-zadeh, Density estimation of pure carbon dioxide at supercritical region and estimation solubility of solid compounds in supercritical carbon dioxide: correlation approach based on sensitivity analysis, *Fluid Phase Equilib.*, 342 (2013) 31–41.
- [36] A. Saltelli, M. Ratto, T. Andres, F. Campolongo, J. Cariboni, D. Gatelli, M. Saisana, S. Tarantola, *Global Sensitivity Analysis: The Primer*, John Wiley & Sons, Chichester, 2008.